Forming Limits of a Sheet Metal After Continuous-Bending-Under-Tension Loading

Ji He
Shanghai Key Laboratory of Digital Manufacture for Thin-Walled Structures, Shanghai Jiao Tong University, Shanghai 200240, PRC

Z. Cedric Xia[1]
e-mail: zxia@ford.com

Danielle Zeng
Ford Motor Company, Dearborn, MI 48121

Shuhui Li
Shanghai Key Laboratory of Digital Manufacture for Thin-walled Structures, Shanghai Jiao Tong University, Shanghai 200240, China; State Key Laboratory of Mechanical System and Vibration, Shanghai 200240, PRC

Forming limit diagrams (FLD) have been widely used as a powerful tool for predicting sheet metal forming failure in the industry. The common assumption for forming limits is that the deformation is limited to in-plane loading and through-thickness bending effects are negligible. In practical sheet metal applications, however, a sheet metal blank normally undergoes a combination of stretching, bending, and unbending, so the deformation is invariably three-dimensional. To understand the localized necking phenomenon under this condition, a new extended Marciniak–Kuczynski (M–K) model is proposed in this paper, which combines the FLD theoretical model with finite element analysis to predict the forming limits after a sheet metal undergoes under continuous-bending-under-tension (CBT) loading. In this hybrid approach, a finite element model is constructed to simulate the CBT process. The deformation variables after the sheet metal reaches steady state are then extracted from the simulation. They are carried over as the initial condition of the extended M–K analysis for forming limit predictions. The obtained results from proposed model are compared with experimental data from Yoshida et al. (2005, "Fracture Limits of Sheet Metals Under Stretch Bending," Int. J. Mech. Sci., 47(12), pp. 1885–1986) under plane strain deformation mode and the Hutchinson and Neale's (1978(a), "Sheet Necking—II: Time-Independent Behavior," Mech. Sheet Metal Forming, pp. 127–150) M–K model under in-plane deformation assumption. Several cases are studied, and the results under the CBT loading condition show that the forming limits of post-die-entry material largely depends on the strain, stress, and hardening distributions through the thickness direction. Reduced forming limits are observed for small die radius case. Furthermore, the proposed M–K analysis provides a new understanding of the FLD after this complex bending-unbending-stretching loading condition, which also can be used to evaluate the real process design of sheet metal stamping, especially when the ratio of die entry radii to the metal thickness becomes small. [DOI: 10.1115/1.4023676]

1 Introduction

Forming limit diagrams (FLD) have been an indispensable assessing tool in practical applications to assess sheet metal formability. Due to its important applications, many theoretical and numerical models have been developed in an attempt to provide fundamental understanding of its physical implications and predict FLD from mechanical principles. Most of the models define the forming limits as the onset of localized necking under biaxial deformation, an instability phenomenon. Only in-plane deformations are considered, with the assumption that the sheet metal is undergoing plane stress deformation and without through-thickness bending.

One of the first theoretical models to predict formability of sheet metal was proposed by Hill [1], where it was assumed that the existence of a zero-extension direction is the necessary condition for localized necking to occur, which corresponds to the left-hand side of FLD. After that, Keeler and Backofen [2] conducted extensive forming limit tests and measurements for a wide variety of sheet metals, with focus on different steel grades. They concluded that localized necking is also possible for a sheet metal under biaxial stretching where zero-extension direction does not exist. He promoted the practical use of FLD on die tryout shop as the criterion for checking the potential splits.

To overcome the difficulty of predicting and understanding the localized necking phenomenon under biaxial stretching condition, Marciniak and Kuczynski [3] introduced an initial band of imperfection into the sheet metal in the form of thickness reduction as a tool to trigger the deformation instability. Under such nonhomogeneous assumptions for sheet metal, localization occurs naturally as the sheet deforms under the entire range of biaxial loading, including on the right-hand side of FLD. This line of analysis is often referred as M–K analysis.

Furthermore, Storen and Rice [4] introduced the vertex theory of plasticity into the instability analysis of sheet metal necking, and were able to predict the forming limit over the entire range of the biaxial strain ratios. They showed that the J_2-Deformation theory of plasticity is a simplified version of the vertex theory under certain assumptions.

Both Vertex-theory analysis and M–K models were extended by Hutchinson and Neale in their three papers [5–7]. Referred as the long-wavelength analysis in these papers, the M–K method is further developed by assuming the rotation of weak band in sheet metal when proportional loadings are applied. This development not only unifies the left-hand side and right-hand side of FLD, but also introduces physical-based minimum energy principle in the prediction of formability.

In practical sheet metal applications, the deformation is invariably three-dimensional. A sheet metal blank normally undergoes a combination of stretching, bending, and unbending. Attempts to formulate a forming limit diagram incorporating three-dimensional stress states have been made by various researchers.

McClintock et al. [8] investigated the localized necking phenomenon in plane strain mode under bending moment with constant tension condition. Both isotropic and kinematic hardening models were used in their analysis. Shi and Gerdeen [9] studied the effect of strain gradient and curvature on forming limit diagrams for anisotropic sheets using strain gradient theory. Assempour et al. [10] modified M–K analysis to include the effect of normal stress on the

[1]Corresponding author.

Contributed by the Materials Division of ASME for publication in the Journal of Engineering Materials and Technology. Manuscript received November 2, 2012; final manuscript received January 7, 2013; published online May 8, 2013. Assoc. Editor: Tetsuya Ohashi.

prediction of the forming limit diagrams. Eyckens et al. [11] proposed an extended M–K model for anisotropic sheet subjected to monotonic strain paths with through-thickness shear. More generally, Triantafyllidis [12] and Triantafyllidis et al. [13] studied the development of shear bands in a plate subject to pure bending. Allwood and Shouler [14] proposed a generalized forming limit diagrams model with nonplanar stress states for incremental forming process, which showed a significantly increased formability. Xia and Zeng [15] proposed a forming limit under stretch-bending theoretical prediction model based on the instability analysis using deformation theory.

However, quantitative predictions remain elusive as compared to a body of work on the experimental front [16–19], especially when the bending radius is small relative to the thickness of the sheet metal.

With increasingly extensive use of higher strength steels in automobiles for weight reductions, more accurate forming limits are needed due to the decreased formability of higher-strength steels for assessing the forming process and die design. The bending effect becomes especially important. Furthermore, smaller die radius is preferred in die and punch design to reduce springback, which in turn results in more significant bending effect.

The motivation of this paper is to build on this insight and extend the M–K analysis incorporated with finite element model for the prediction of the right-hand side FLD after the sheet metal undergoes continuous-bending-under-tension (CBT) deformation. We focus our attention on the forming limits where the bending is limited to the direction of major strain. The objective is to provide a framework for the understanding of CBT effect on FLD and the prediction of CBT-FLD for post-die-entry sheet metal.

In this study, a sheet metal flowing through the different die radii is constructed in the finite element analysis (FEA) model. The metal flow is limited to one loading direction while the minor principal loading direction is assumed to deform under the plane strain condition. After the sheet metal completely goes through the die radius, the complete deformation state including strains, stresses and hardening conditions across the thickness direction are extracted from the FEA results. They are, in turn, used as the starting input of the extended M–K analytical analysis. As a matter of fact, only the right-hand side of FLD is investigated in this paper, and the plasticity theory with associated flow rule is adopted to describe material deformation behavior under the continuous-bending-under-tension loading. It should also be noted that material unloading and reverse loading are inherently a part of the deformation process.

The obtained results from the proposed model show that CBT process has a substantial impact on the formability of the post-die-entry sheet metal due to nonuniform distributions of strain, stress, and hardening conditions across the sheet thickness. For practical applications, the sheet metal in general undergoes multiple bending, unbending, and stretching deformations, and it will have significant impact on the final formability of the sheet metal.

2 Outline of the Technical Approach

When a sheet metal flows through the die radii in a real-world sheet metal forming process, it undergoes continuous deformation such as bending, unbending and stretching. Complex deformation state is thus introduced with nonuniform stresses and strains across metal thicknesses, contrary to in-plane deformation assumptions that conventional FLDs are based.

The Marciniak-Kuczynski (M–K) model has proved to be a powerful tool in analyzing forming limits under complex loading conditions and understanding major factors in influencing forming limits. In a sister paper [20] an extended M–K method was developed to study the forming limits under the condition of stretch-bending. The same approach can be adopted in principle to investigate forming limits under CBT loading considered here. However, the deformation history when a sheet metal goes through a die entry radius is a much more complicated contact problem, and analytical solutions are not readily available. To this end, a hybrid approach is established here and it is outlined here as a three-step process:

Firstly, a finite element model is constructed to simulate the continuous-bending-under-tension process with a sheet metal being pulled through a die entry radius. Simulation results for a range of die entry radii can be readily obtained. We are interested in the steady-state deformation results after the material completely passes through the die radius.

Secondly, the simulation results for the steady-state deformation are extracted. The results include all deformation variables, including stresses, plastic strains, and all state variables across the sheet metal thickness as well as current metal thickness.

Lastly, the extracted deformation results at the end of CBT loading are carried over as the initial condition to M–K analysis. A band of pre-existing imperfection in the form of a slightly smaller thickness is introduced to enable the occurrence of localized necking. Different strain paths are applied to cover the entire range of the right-hand side FLD.

The flow chart in Fig. 1 illustrates the main framework of this hybrid approach.

3 Finite Element Model

For simplicity, the CBT loading process is assumed under plane strain condition, which is consistent with the draw-bend test assumptions in experiment. The numerical simulation is conducted with commercial FEM software Abaqus/Standard, and the shell element S4R is chosen. Frictions are ignored in the FE model since they do not fundamentally change the deformation behavior. The punch and die are assumed to be rigid for the purpose of this simulation. The 9-point Gaussian method is used in the shell

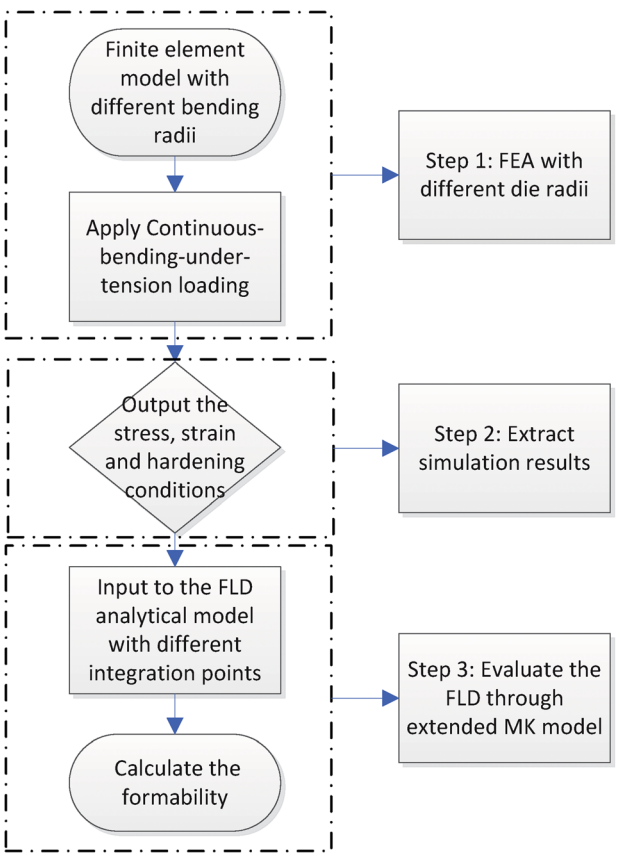

Fig. 1 Framework of the hybrid approach to evaluate the forming limits of CBT loading

element for through-thickness integration, and a mesh size of 0.1 mm is adopted in the model. Finer mesh size and more integration points are also investigated but simulation results remain essentially the same. Hill'48 yielded a surface with transversely isotropic r-values and isotropic hardening is assumed. The swift equation of Eq. (1) is used for the effective stress-strain relationship, the parameters of which are obtained from uniaxial tension test,

$$Y(\varepsilon_e) = K(\varepsilon_0 + \varepsilon_e)^n \tag{1}$$

The material parameters of DP600 are employed in this model. ε_0 is initial elastic limit strain, which is valued as 0.002, K and n are set as 945.5 and 0.22 in this study, and ε_e is defined as the equivalent plastic strain.

A schematic setup for the sheet metal under CBT loading action is illustrated in Fig. 2, where t_0 represents the initial thickness of the sheet metal with a fixed value 1.0 mm in the FE model. R is the die radius for the sheet metal drawing process which is chosen as 5, 10, and 50 mm in the FE model. As the sheet metal flows through the die radius it is bent and stretched. It is then straightened again under reverse bending moment when it is in the existing radius area. After the material completely undergoes the bending, unbending, and stretching processes and reaches steady-state deformation, deformation results from one section across the thickness are extracted as the starting point of M–K analysis.

It should be noted that the above model ignored the frictional effect and also does not contain any back forces in order to simplify the complexity of the problem. Such frictional effect and back-force effect can be easily incorporated in the model to more closely reflect actual problems encountered in practical applications.

4 Forming Limit Analysis After CBT Loading

4.1 Assumptions. In present study, the M–K model is generalized to three-dimensional with deformation variables distributed across metal thickness through Gaussian integration points. It enables the inclusion of the complex CBT effect on the forming limits. The deformation state of each material point at the start of M–K analysis is carried over from FEA simulations. Biaxial loading is then applied to the sheet metal with the same incremental in-plane strains at all material points through thickness.

As stated earlier, an imperfection region is introduced in the sheet metal to facilitate the localization. As customary in conventional M–K analysis, it is denoted as region "b" while the normal area as region "a." For both the normal area "a" and defect area "b," two necessary conditions, known as compatibility and equilibrium are satisfied across the imperfection boundary, which can be expressed as

$$F_x^a = F_x^b \tag{2}$$

$$\Delta\varepsilon_y^a = \Delta\varepsilon_y^b \tag{3}$$

On the right-hand quadrant of the forming limit diagram, the imperfection band is always perpendicular to the major strain direction. Since only the right-hand side of the FLD is studied as stated earlier, both the strain of X and Y directions in this side are positive.

4.2 Flow Theory Based Model. For the sake of simplicity and consistency, the isotropic hardening assumption and Hill'48 yield surface are adopted in this analysis for both region a and b, which are defined as

$$Y((\varepsilon_e)_{\xi_i}) = K(\varepsilon_0 + (\varepsilon_e)_{\xi_i})^n \tag{4}$$

$$f(\boldsymbol{\sigma}_{\xi_i}) = \sqrt{(\sigma_x^2)_{\xi_i} - \frac{2r}{1+r}(\sigma_x)_{\xi_i}(\sigma_y)_{\xi_i} + (\sigma_y^2)_{\xi_i} + \frac{2(1+r)}{1+r}(\sigma_{xy}^2)_{\xi_i}} \tag{5}$$

The effective plastic strain at each Gaussian point ξ_i is expressed as $(\varepsilon_e)_{\xi_i}$. The same also applies to stress quantities $(\sigma_x)_{\xi_i}$, $(\sigma_y)_{\xi_i}$, and $(\sigma_{xy})_{\xi_i}$. The initial values of those variables are based on the output of the finite element model under the corresponding ratio of radius and thickness. This also applies to materials at both regions a and b.

According to Xia [21], the Hill'48 yield criterion also takes the form,

$$f(\boldsymbol{\sigma}_{\xi_i}) = \sqrt{\frac{3}{2}\boldsymbol{\sigma}_{\xi_i}^T P \boldsymbol{\sigma}_{\xi_i}} - Y((\varepsilon_e)_{\xi_i}) \tag{6}$$

where $\mathbf{P}$ is the anisotropic plasticity matrix. For transversely isotropic yield with an average r-value, it is given by, under plane stress condition,

$$\mathbf{P} = \frac{2}{3}\begin{bmatrix} 1 & -\frac{r}{1+r} & 0 \\ -\frac{r}{1+r} & 1 & 0 \\ 0 & 0 & \frac{2(1+2r)}{1+r} \end{bmatrix} \tag{7}$$

The imperfection index can be defined with the thickness t_0 and $\hat{t}_0$ of regions a and b, respectively,

$$\zeta = \left(1 - \frac{\hat{t}_0}{t_0}\right) \tag{8}$$

Throughout the analysis a superscript ^ will denote quantities in the groove (region b) of the sheet metal whereas the absence of this symbol will refer to quantities associated with behavior in the normal region (region a). The values of z are chosen as the positions of material points through the thickness on the Z axis.

Now M–K model analysis is applied to the CBT-affected sheet metal. As outlined earlier, the stress, strain, and plasticity state variable results as well deformed metal thickness of the last step in FE analysis become the starting point for the necking analysis process. Since the defect band is always perpendicular to the major strain direction, the strain increment matrix can be defined as

$$\Delta\varepsilon = \begin{bmatrix} \Delta\varepsilon_x \\ \Delta\varepsilon_y \end{bmatrix} \tag{9}$$

$$\Delta\hat{\varepsilon} = \begin{bmatrix} \Delta\hat{\varepsilon}_x \\ \Delta\hat{\varepsilon}_y \end{bmatrix} \tag{10}$$

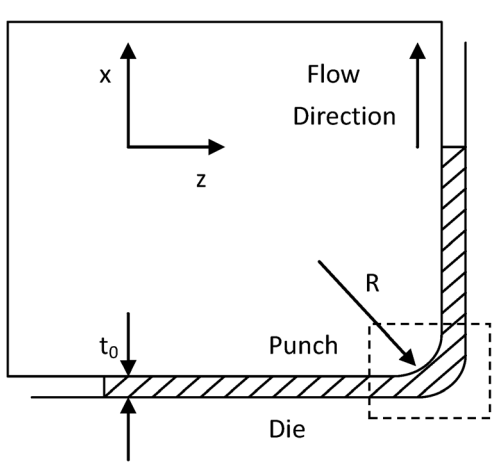

Fig. 2 The schematic setup for the CBT loading process

where $\Delta\varepsilon_x$, $\Delta\hat{\varepsilon}_x$ are average tension strain increments in the two regions of the sheet. They are related to $\Delta\varepsilon_y$, $\Delta\hat{\varepsilon}_y$ through

$$\rho = \frac{\Delta\varepsilon_y}{\Delta\varepsilon_x} \tag{11}$$

$$\Delta\varepsilon_y = \Delta\hat{\varepsilon}_y \tag{12}$$

where ρ is the strain ratio ranging from 0 to 1, corresponding to the right-hand side of FLD.

For one incremental step loading, the strains can be expressed as

$$\boldsymbol{\varepsilon}^{T+\Delta T} = \boldsymbol{\varepsilon}^{T} + \Delta\boldsymbol{\varepsilon} \tag{13}$$

$$\hat{\boldsymbol{\varepsilon}}^{T+\Delta T} = \hat{\boldsymbol{\varepsilon}}^{T} + \Delta\hat{\boldsymbol{\varepsilon}} \tag{14}$$

Thus, the stress conditions at time step $T+\Delta T$ and T are given as

$$(\boldsymbol{\sigma}^{T+\Delta T})_{\xi_i} = (\boldsymbol{\sigma}^{*})_{\xi_i} - \mathbf{D}(\Delta\boldsymbol{\varepsilon}^{pl})_{\xi_i} \tag{15}$$

$$(\hat{\boldsymbol{\sigma}}^{T+\Delta T})_{\xi_i} = (\hat{\boldsymbol{\sigma}}^{*})_{\xi_i} - \mathbf{D}(\Delta\hat{\boldsymbol{\varepsilon}}^{pl})_{\xi_i} \tag{16}$$

$$(\boldsymbol{\sigma}^{*})_{\xi_i} = (\boldsymbol{\sigma}^{T})_{\xi_i} + \mathbf{D}\Delta\boldsymbol{\varepsilon} \tag{17}$$

$$(\hat{\boldsymbol{\sigma}}^{*})_{\xi_i} = (\hat{\boldsymbol{\sigma}}^{T})_{\xi_i} + \mathbf{D}\Delta\hat{\boldsymbol{\varepsilon}} \tag{18}$$

Here $\mathbf{D}$ is the elastic matrix. From expressions (17) and (18) above, two trial stresses are substituted into yield surface criterion to check whether the material will be deformed elastically or plastically. If under plastic yielding, the radial return method is employed to integrate the plastic flow in conjunction with the associated flow rule. Equations for plastic deformation can be obtained as follows:

$$(\boldsymbol{\sigma}^{T+\Delta T})_{\xi_i} = \left(\mathbf{I} + (\Delta\varepsilon_e)_{\xi_i}\frac{3}{2Y((\varepsilon_e)_{\xi_i}^{T+\Delta T})}\mathbf{DP}\right)^{-1}((\boldsymbol{\sigma}^{T})_{\xi_i} + \mathbf{D}\Delta\boldsymbol{\varepsilon}) \tag{19}$$

$$(\hat{\boldsymbol{\sigma}}^{T+\Delta T})_{\xi_i} = \left(\mathbf{I} + (\Delta\hat{\varepsilon}_e)_{\xi_i}\frac{3}{2Y((\hat{\varepsilon}_e)_{\xi_i}^{T+\Delta T})}\mathbf{DP}\right)^{-1}((\hat{\boldsymbol{\sigma}}^{T})_{\xi_i} + \mathbf{D}\Delta\hat{\boldsymbol{\varepsilon}}) \tag{20}$$

$$f(\boldsymbol{\sigma}^{T+\Delta T})_{\xi_i} = \sqrt{\frac{3}{2}(\boldsymbol{\sigma}^{T+\Delta T})_{\xi_i}\mathbf{P}(\boldsymbol{\sigma}^{T+\Delta T})_{\xi_i}} - Y((\varepsilon_e)_{\xi_i}^{T+\Delta T}) = 0 \tag{21}$$

$$f((\hat{\boldsymbol{\sigma}}^{T+\Delta T})_{\xi_i}) = \sqrt{\frac{3}{2}(\hat{\boldsymbol{\sigma}}^{T+\Delta T})_{\xi_i}\mathbf{P}(\hat{\boldsymbol{\sigma}}^{T+\Delta T})_{\xi_i}} - Y((\hat{\varepsilon}_e)_{\xi_i}^{T+\Delta T}) = 0 \tag{22}$$

where $(\varepsilon_e)_{\xi_i}^{T+\Delta T}$, $(\hat{\varepsilon}_e)_{\xi_i}^{T+\Delta T}$ can be expressed as

$$(\varepsilon_e)_{\xi_i}^{T+\Delta T} = (\varepsilon_e)_{\xi_i}^{T} + (\Delta\varepsilon_e)_{\xi_i} \tag{23}$$

$$(\hat{\varepsilon}_e)_{\xi_i}^{T+\Delta T} = (\hat{\varepsilon}_e)_{\xi_i}^{T} + (\Delta\hat{\varepsilon}_e)_{\xi_i} \tag{24}$$

Both equivalent plastic strains in two regions are accumulated with the hardening effect step by step.

Then, with the relevant Gaussian weights w_i and the number of integration points (NIP), we have

$$F_x^a = \frac{t}{2}\cdot\sum_{i=1}^{\mathrm{NIP}} w_i\cdot(\sigma_x)_{\xi_i} \tag{25}$$

$$F_x^b = \frac{\hat{t}}{2}\cdot\sum_{i=1}^{\mathrm{NIP}} w_i\cdot(\hat{\sigma}_x)_{\xi_i} \tag{26}$$

$$\sum_{i=1}^{\mathrm{NIP}} w_i\cdot(\sigma_x)_{\xi_i} = \left(\frac{\hat{t}}{t}\right)\cdot\sum_{i=1}^{\mathrm{NIP}} w_i\cdot(\hat{\sigma}_x)_{\xi_i} \tag{27}$$

If the above equations are rearranged, the model can be expressed as

$$\begin{cases} f((\hat{\boldsymbol{\sigma}}^{T+\Delta T})_{\xi_1}) - Y((\hat{\varepsilon}_e)_{\xi_1}^{T+\Delta T}) = 0 \\ f((\hat{\boldsymbol{\sigma}}^{T+\Delta T})_{\xi_2}) - Y((\hat{\varepsilon}_e)_{\xi_2}^{T+\Delta T}) = 0 \\ \vdots \\ f((\hat{\boldsymbol{\sigma}}^{T+\Delta T})_{\xi_i}) - Y((\hat{\varepsilon}_e)_{\xi_i}^{T+\Delta T}) = 0 \\ \sum_{i=1}^{\mathrm{NIP}} w_i\cdot(\sigma_x)_{\xi_i} = \left(\frac{\hat{t}}{t}\right)\cdot\sum_{i=1}^{\mathrm{NIP}} w_i\cdot(\hat{\sigma}_x)_{\xi_i} \end{cases} \tag{28}$$

By now, the numerical solution can be obtained through the Newton–Raphson method.

The criterion for detecting the localized necking strain is such that the average incremental tension strain ratio of inside and outside the groove reaches

$$\frac{\Delta\hat{\varepsilon}_x}{\Delta\varepsilon_x} \geq 10 \tag{29}$$

5 Results and Discussion

5.1 Results From Finite Element Models. To fully understand the deformation behavior under CBT loading, we follow a section of the sheet metal through its deformation history and examine its stress and strain evolutions. With nine Gaussian integration points being employed across the thickness in the model, we can trace each of them and get a full picture of the metal deformation. Since every section of the sheet metal experiences the same deformation when passing through the die radius, we only need to focus on one section throughout its deformation history. R/t_0, the ratio of die radius to metal thickness, will influence the magnitude of the deformation, but the behavior is qualitatively same. Both the stress and strain conditions are recorded at each Gaussian point across the thickness and throughout the deformation history (Fig. 3).

The typical strain evolution phenomenon under the $R/t_0 = 5$ condition is shown in Fig. 4, where the X axis is along the material flow direction. It is evident that the existence of significant strain differential across metal thickness due to the bending strain under the bending process, followed by the unbending process where the strains across the thickness become more or less equal as the sheet metal gets straightened. The stretch process adds a tensile

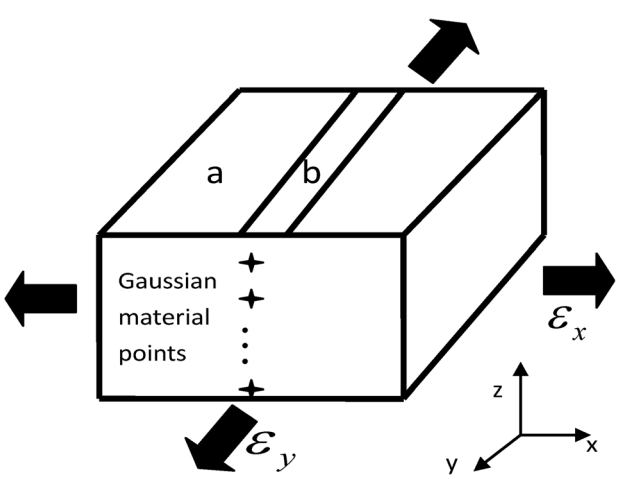

Fig. 3 Schematic diagram of Gaussian material points through the thickness direction

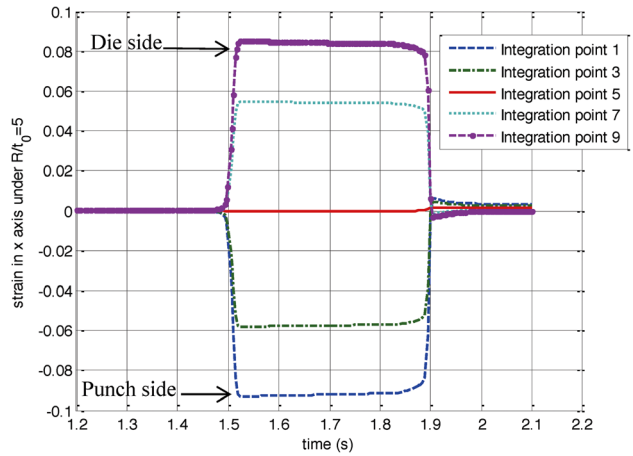

Fig. 4 The strain distribution through thickness direction after the material undergoes the die radius with $R/t_0 = 5$

component to their major strains across the thickness, which is consistent with the experimental observation and understanding.

The stress evolution for $R/t_0 = 5$ is shown in Fig. 5. The deformation history is more complex because of the loading/unloading behavior. The sheet metal is bent when it enters the die radius, resulting in compression stress on one side of the surface and tensile stress on another side. It is then bent back when it passes through the die radius exit and becomes stretched almost uniformly in the X axis direction, which reverses the stress conditions across the sheet thickness and shifts the stress of middle material layer to tension.

Since there is no friction assumed in the FE model during the deformation process, the selected section surface force comes from the contact between the sheet metal and the die. As shown in Fig. 6, increased R/t_0 value provides elevated section force in the X axis direction, which means it imposes more stretch strains in the sheet metal.

5.2 Validation of Forming Limit Prediction

5.2.1 M–K Model Validation for In-Plane Deformation. First of all, the M–K analysis we developed is validated under in-plane deformation assumption for conventional FLD. Hutchinson and Neale [5] flow theory based long-wavelength (M–K) analysis under no bending effect is chosen to compare the results on the right-hand quadrant. For the purpose of consistency, the material parameters in proposed model is set at $K = 945.5$ MPa, $\zeta = 0.01$,

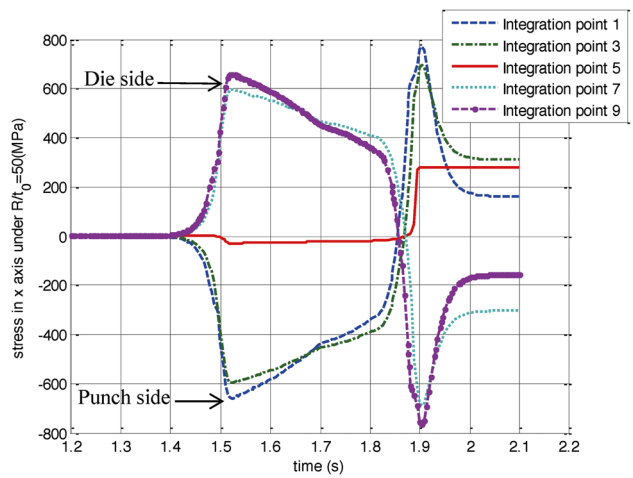

Fig. 5 The stress distribution through thickness direction after the material undergoes the die radius with $R/t_0 = 5$

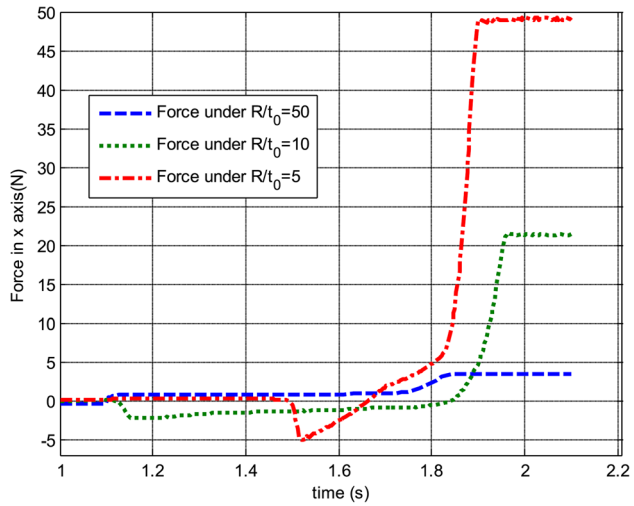

Fig. 6 The force evolution under three different R/t_0 values in the *x* axis direction

$\varepsilon_0 = 0.002$, and the r-value $= 1$. Since no bending effect existed in conventional M–K analysis, the initial stress, strain, and hardening conditions are valued as zero and no FE model is constructed before analysis.

As shown in Fig. 7, it seems that the four curves from those different models are perfectly fit with each other with the same material mechanical properties description. Figure 12, below, provides at least partial validation of algorithms and accuracy of the developed model.

5.2.2 M–K Model Validation Under Plane Strain Condition From the Theoretical Side. According to the maximum force criterion in Eq. (30), which was used by pioneer researcher McClintock et al. [8], the FLD_0 values under the plane strain deformation mode are examined at first with different imperfection sizes in proposed M–K analysis, where R/t_0 ranged from 5, 10, 50 to 1000, n-value $= 0.22$, $\varepsilon_0 = 0.002$, and r-value $= 1$. As stated earlier, when R/t_0 equals 1000 in our analysis, the initial stress, strain, and hardening conditions are valued as zero and no FE model is constructed,

$$\frac{\partial F_x}{\partial \varepsilon_x} = 0 \tag{30}$$

The results in Fig. 8 show the same trend of the CBT loading effect on FLD_0 values, which clearly decreases the FLD_0 rapidly

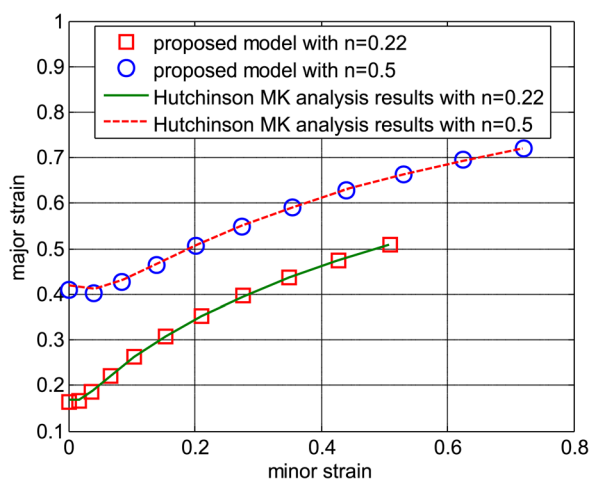

Fig. 7 The validation of the extended M–K analysis model

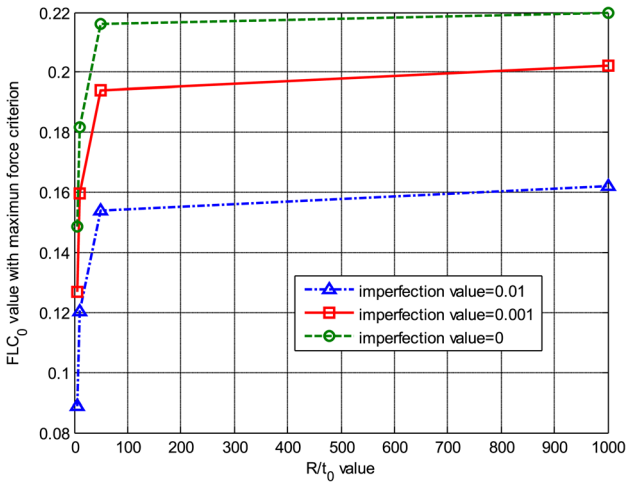

Fig. 8 FLD_0 values under the *n*-value = 0.22 and three different imperfection conditions

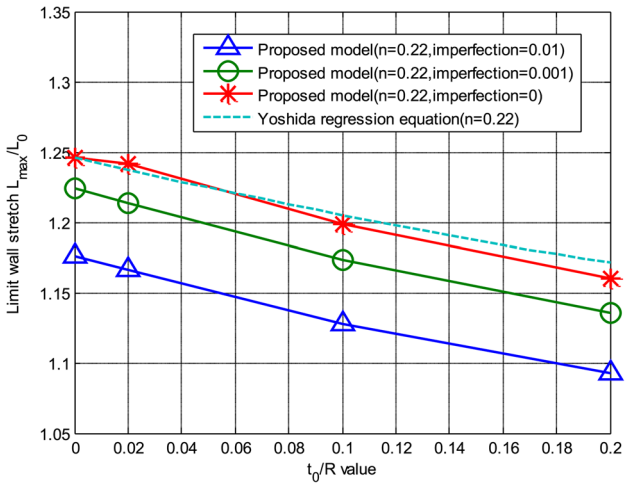

Fig. 10 FLD_0 values under the *n*-value = 0.22 of proposed model compared with the Yoshida's regression equation with the same *n*-value

in small R/t_0 values and seems to have no significant effect on the large R/t_0 values range. If the curve of the large imperfection size shifts upward, the three curves can fit with each other reasonably.

5.2.3 M–K Model Validation Under Plane Strain Condition From the Experimental Side. Similar trends of experimental results can be observed in Yoshida et al. [22]; their experiments were also performed and based on the plane strain mode named three-point stretch bending test. The schematic of the stretch bending test is presented in Fig. 9. The aluminum material 5182-O (n-value = 0.233) was used to construct the experiment with both $L_0 = 118.4$ mm and $L_0 = 69.8$ mm. Similarly, the ratio between initial thickness t_0 of the sheet and punch radius R are used as a nondimensional bending index t_0/R. The limit wall stretch is used to value the ability of the maximum stretch length L_{max} for different L_0 sheet metals. The results under plane strain mode from the new proposed model with fixed n-value = 0.22, $K = 945.5$ MPa, $\varepsilon_0 = 0.002$, and r-value = 1 parameters are compared with Yoshida's experimental data from their original paper in Fig. 11 below.

In their paper, Yoshida et al. [22] proposed the following regression equation based on their numerical model and experimental results:

$$\frac{L_{max}}{L_0} = e^n + (1 - e^n)(1 - e^{-(0.4/n)(t_0/R)}) \tag{31}$$

This equation fit the experimental data very well. Figure 10 shows the comparison between the proposed model and Yoshida's equation with the same n-value under the plane strain condition. The

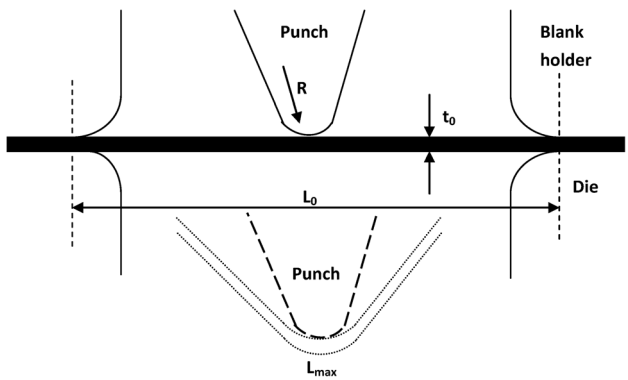

Fig. 9 The schematic of stretch bending test

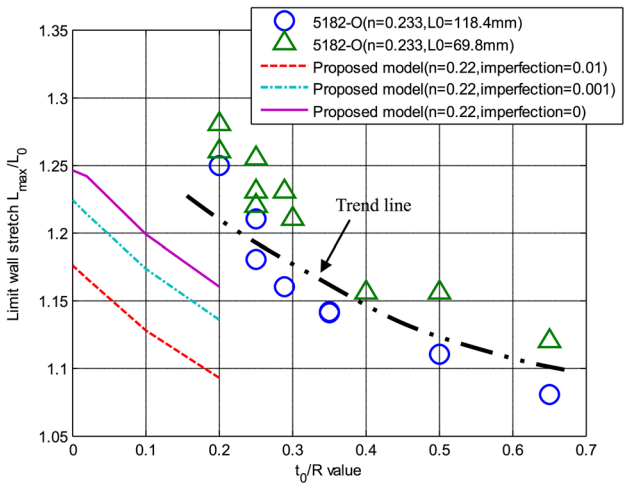

Fig. 11 FLD_0 values under the *n*-value = 0.22 of proposed model compared with the experimental results from Yoshida's paper

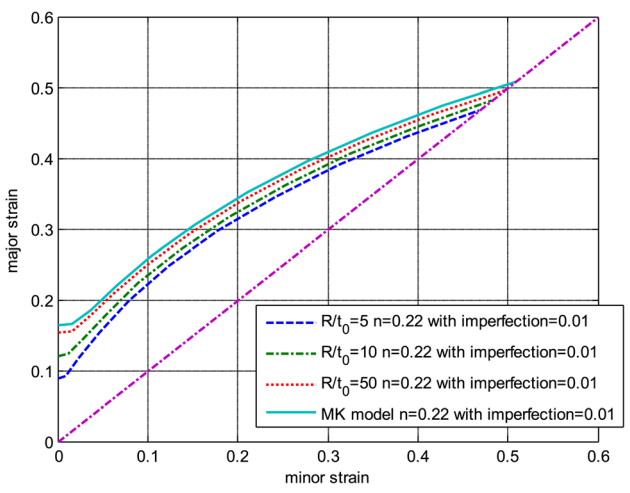

Fig. 12 Forming limit diagram on the right-hand side under the CBT loading condition with imperfection equal to 0.01

same trend can be found in Fig. 10, and the curve under the imperfection = 0 condition calculated through the maximum force criterion (as stated in Sec. 5.2.2) seems very close to the results from Yoshida's equation.

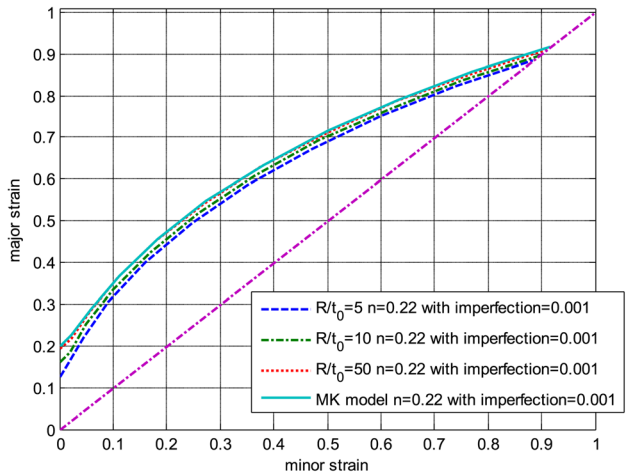

Fig. 13 Forming limit diagram on the right-hand side under the CBT loading condition with imperfection equal to 0.001

The experimental results are compared with our model in Fig. 11. The t_0/R value is decreasing with the limit wall stretch in Fig. 11, and the same trend of the t_0/R value effect can be clearly observed here, which provides another validation from the experimental side under plane strain condition of the developed model. The different n-value in model and stretch-bending-test material may be the source for the small gap between the expected curves and experimental data.

5.3 FLD Results From the Theoretical Model. Figures 12 and 13 show the results on right-hand side of the FLD, which is based on the different imperfection sizes, but the same material parameters, such as n-value $= 0.22$, $\varepsilon_0 = 0.002$, r-value $= 1$, and $K = 945.5$ MPa. It seems that the more CBT loading effect imposed to the sheet metal the lower forming limits it can provide. When we compare Figs. 12 and 13 at the same time, it is clear that this kind effect is smaller under the $\zeta = 0.001$ condition than $\zeta = 0.01$.

From Figs. 4 and 5 we can find that when the sheet metal flows through the die radius under CBT loading condition, the strain

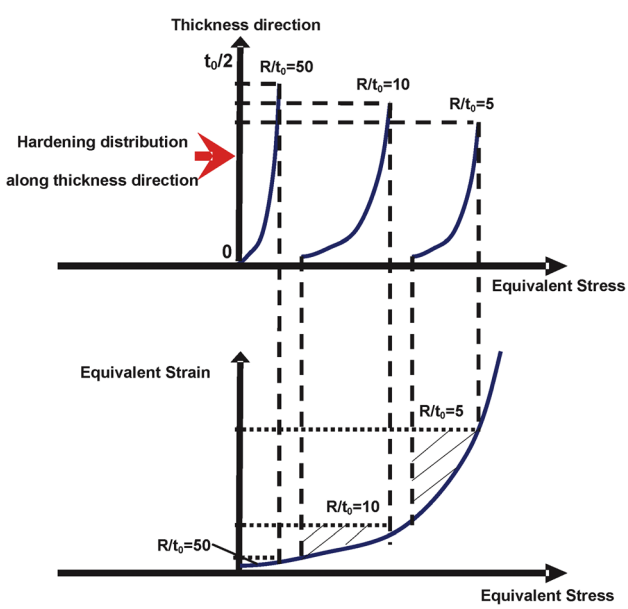

Fig. 14 Illustration of the hardening distribution along the thickness direction after the CBT loading condition for R/t_0 equal to 50, 10, and 5

and stress distribution changes a lot following with the different hardening effect on different material layers across the thickness direction.

With the different hardening distribution across the thickness direction after the CBT loading condition as illustrated in Fig. 14, we can understand that the higher R/t_0 ratio gives the higher hardening condition in the sheet which reduces the ability of necking resistance. The "harder" the material becomes, the lower forming limits present, which illustrates the relationship between the hardening condition and forming limit of the material under the CBT loading process. As a result, the accelerated necking phenomenon can be observed through CBT loading condition in the sheet metal deformation process.

6 Conclusions

A hybrid approach to evaluate the forming limits of a sheet metal after CBT loading has been proposed in this paper. It combines a finite element analysis for the CBT process with a newly extended M–K model incorporating through-thickness deformation. The results are first validated for in-plane deformations against Hutchinson and Neale [5] long-wavelength (M–K) analysis on the right-hand side. Furthermore, the experimental data under the plane strain deformation mode of the aluminum material 5182-O from Yoshida et al. [22] is used to compare the predicted results, and the same trend is observed based on the different material parameters. Yoshida's regression equation, which is based on his numerical model and experiment, is used to compare the results of our model with the same material parameters, and good agreement is found under imperfection equal to 0. These results are consistent with our expectations. All of the validations presented above are partially confirmed with the newly proposed M–K analysis in this paper.

If we set the initial input of stress, strain, and hardening conditions after the CBT loading as zero, the conventional FLD on right-hand side can be achieved. Here, the common understanding of FLD without bending effect is unified with the proposed CBT-FLD for post-die-entry sheet metal. Furthermore, by using the extended understanding from the CBT-FLD model, the stress, strain, and hardening conditions across the thickness direction are related with the forming limits under the continuous-bending-under-tension process. This kind effect clearly decreases the FLD of the post-die-entry material. It seems FLD is less sensitive in small imperfection size, but the case is not true in big imperfection situation. This CBT-FLD model also can be used for evaluating the real process design of sheet metal stamping, especially for the die-corner fracture. The extended M–K analysis provides a consistent way to understand the localized necking phenomenon under the three-dimensional loading condition, where only one bending moment along the major loading direction is imposed.

It should be noted that the constitutive model employed in the current study is the Hill'48 yield surface with transversely isotropic r-values and isotropic hardening. Previous studies show that the forming limit prediction is fairly sensitive to the material models used. It will be of interest to extend the current framework to other models.

(1) Nonquadratic yield surface models. Banabic et al. [23] provides an excellent review of the recently developed advanced yield surface models. They should be readily applicable under the framework developed in this paper. It will be interesting to see how these models will affect the prediction of forming limits with continuous bending-under-tension loading. Careful examinations should also be paid to investigate the necking orientation when material anisotropy is present.

(2) Anisotropic hardening models where kinematic hardening is accounted for. Since the sheet metal undergoes multiple loading-unloading-reverse loading during continuous bending-under-tension deformation, the predicted stress state

after such deformation will be significantly affected by the hardening models used in the simulation. Therefore, it is expected that the predicted forming limits will show some sensitivity. Further studies will clarify their influences.

Acknowledgment

This study is conducted while one of the authors (Ji He) is a visiting academic at the Research and Innovation Center of Ford Motor Company in Dearborn, Michigan. Financial support from National Natural Science Foundation of China (51222505) and Ford Motor Company through its University Research Program (URP) is gratefully acknowledged.

References

[1] Hill, R., 1952, "On Discontinuous Plastic States, With Special Reference to Localized Necking in Thin Sheets," J. Mech. Phys. Solids, **1**(1), pp. 19–30.
[2] Keeler, S. P., and Backofen, W. A., 1964, "Plastic Instability and Fracture in Sheets Stretched Over Rigid Punches," ASM Trans. Quart., **65**, p. 25.
[3] Marciniak, Z., and Kuczynski, K., 1967, "Limit Strains in the Processes of Stretch-Forming Sheet Metal," Int. J. Mech. Sci., **9**(9), pp. 609–612.
[4] Storen, S., and Rice, J., 1975, "Localized Necking in Thin Sheets," J. Mech. Phys. Solids, **23**(6), pp. 421–441.
[5] Hutchinson, J., and Neale, K., 1978a, "Sheet Necking—II: Time-Independent Behavior," D. P. Koistinen, and N. M. Wang, eds., *Mechanics of Sheet Metal Forming*, Plenum Press, New York, pp. 127–150.
[6] Hutchinson, J., and Neale, K., 1978b, "Sheet Necking—III: Strain-Rate Effects," D. P. Koistinen, and N. M. Wang., eds., *Mechanics of Sheet Metal Forming*, Plenum Press, New York, pp. 269–285.
[7] Hutchinson, J., Neale, K., and Needleman, A., 1978c, "Sheet Necking—I: Validity of Plane Stress Assumptions of the Long-Wavelength Approximation," D. P. Koistinen, and N. M. Wang, eds., *Mechanics of Sheet Metal Forming*, Plenum Press, New York, pp. 111–126.
[8] McClintock, F. A., Zhou, Q., and Wierzbick, T., 1993, "Necking in Plane Strain Under Bending With Constant Tension," J. Mech. Phys. Solids, **41**(8), pp. 1327–1343.
[9] Shi, M., and Gerdeen, J., 1991, "Effect of Strain Gradient and Curvature on Forming Limit Diagrams for Anisotropic Sheets," J. Mater. Shaping Technol., **9**(4), pp. 253–268.
[10] Assempour, A., Nejadkhaki, H. K., and Hashemi, R., 2010, "Forming Limit Diagrams With the Existence of Through-Thickness Normal Stress," Comput. Mater. Sci., **48**(3), pp. 504–508.
[11] Eyckens, P., Van Bael, A., and Van Houtte, P., 2011, "An Extended Marciniak-Kuczynski Model for Anisotropic Sheet Subjected to Monotonic Strain Paths With Through-Thickness Shear," Int. J. Plast., **27**(10), pp. 1577–1597.
[12] Triantafyllidis, N., 1980, "Bifurcation Phenomena in Pure Bending," J. Mech. Phys. Solids, **28**(3–4), pp. 221–245.
[13] Triantafyllidis, N., Needleman, A., and Tvergaard, V., 1982, "On the Development of Shear Bands in Pure Bending," Int. J. Solids Struct., **18**(2), pp. 121–138.
[14] Allwood, J. M., and Shouler, D. R., 2009, "Generalised Forming Limit Diagrams Showing Increased Forming Limits With Non-Planar Stress States," Int. J. Plast., **25**(7), pp. 1207–1230.
[15] Xia, Z. C., and Zeng, D., 2008, "Sheet Metal Forming Limit Under Stretch-Bending," ASME International Manufacturing Science and Engineering Conference (ICMP2008), Evanston, IL, October 7–10, ASME Paper No. ICMP2008-72555, pp. 661–667.
[16] Tharrett, M., and Stoughton, T., 2003, "Stretch-Bend Forming Limits of 1008 AK Steel, 70/30 Brass, and 6010 Aluminum," Tenth International Symposium on Plasticity and its Current Applications (PLASTICITY'03), Quebec, Canada, July 7–11, pp. 199–201.
[17] Tharrett, M. R., and Stoughton, T. B., 2003, "Stretch-Bend Forming Limits of 1008 AK Steel," SAE Technical Paper 2003-01-1157.
[18] Kitting, D., Koplenig, M., Ofenheimer, A., Pauli, H., and Till, E., 2009, "Application of a 'Concave-Side Rule' Approach for Assessing Formability of Stretch-Bent Steel Sheets," Int. J. Mater. Forming, **2**, pp. 427–430.
[19] Kitting, D., Ofenheimer, A., Pauli, H., and Till, E., 2010, "A Phenomenological Concept to Predict Formability in Stretch-Bending Forming Operations," Int. J. Mater. Forming, **3**, pp. 1163–1166.
[20] He, J., Xia, Z. C., Li, S. H., and Zeng, D., 2013, "M–K Analysis of Forming Limit Diagram Under Stretch-Bending," ASME J. Manuf. Sci. Eng. (submitted).
[21] Xia, Z. C., 2001, "Failure Analysis of Tubular Hydroforming," ASME J. Eng. Mater. Technol., **123**(4), pp. 423–429.
[22] Yoshida, M., Yoshida, F., Konishi, H., and Fukumoto, K., 2005, "Fracture Limits of Sheet Metals Under Stretch Bending," Int. J. Mech. Sci., **47**(12), pp. 1885–1896.
[23] Banabic, D., Barlat, F., Cazacu, O., and Kuwabara, T., 2010, "Advances in Anisotropy and Formability," Int. J. Mater. Forming, **3**, pp. 165–189.